Published in final edited form as:
Environ Toxicol Chem. 2019 April ; 38(4): 820–830. doi:10.1002/etc.4367.

A 72-hour exposure study with Eastern oysters, *Crassostrea virginica*, and the

Bushra Khan[a,*], **Adeyemi S. Adeleye**[a,†], **Robert M. Burgess**[b], **Roxanna Smolowitz**[c], **Stephen M. Russo**[d], and **Kay T. Ho**[b]

[a]National Research Council Postdoctoral Research Associate, US Environmental Protection Agency, Atlantic Ecology Division, Office of Research and Development, National Health and Environmental Effects Research Laboratory, Narragansett, Rhode Island, USA

[b]US Environmental Protection Agency, Atlantic Ecology Division, Office of Research and Development, National Health and Environmental Effects Research Laboratory, Narragansett, Rhode Island, USA

[c]Roger Williams University, Bristol, Rhode Island, USA

[d]Oak Ridge Associated Universities Student Services Contractor, US Environmental Protection Agency, Atlantic Ecology Division, Office of Research and Development, National Health and Environmental Effects Research Laboratory, Narragansett, Rhode Island, USA

Abstract

Graphene is a two-dimensional nanomaterial with unique mechanical, thermal, electrical, and optical properties. With increasing applications of graphene-family nanomaterials (GFNs) in electronics, biomedicine, and surface coatings, concern for their impacts on aquatic ecosystems is rising. Current information on the toxicity of GFNs, including graphene oxide (GO), is scarce. Filter-feeding bivalves, such as Eastern oysters, are good models for nanomaterial exposure studies. We present results from a 72-hour static renewal oyster study using 1 and 10 mg/L GO which, to our knowledge, is the first report on in vivo effects of GO exposures in marine bivalves. Water samples were analyzed for GO concentration and size assessments. Gill and digestive gland (DG) tissues were evaluated for lipid peroxidation and glutathione-s-transferase (GST) activity. Additionally, gill sections were fixed for histopathological analyses. Elevated lipid peroxidation was noted in oysters exposed to 10 mg/L GO. No significant changes in GST activity were observed, but reduced total protein levels were found in DG tissues of exposed oysters at both concentrations. Loss of mucous cells, hemocytic infiltration, and vacuolation were observed in

[*]corresponding author: Bushra Khan, khan.bushra@epa.gov.
[†]Current address: Department of Civil & Environmental Engineering, University of California, Irvine, CA 92697, USA

DECLARATION OF INTEREST: We declare no conflicts of interest.

This article contains online-only Supplemental Data

DATA ACCESSIBILITY: Readers can access much of the data and associated statistical assessments in the Supplemental Information (SI). Additional data and supporting information are available on request (khan.bushra@epa.gov).

gills of exposed oysters. Results indicate that short-term GO exposures can induce oxidative stress, epithelial inflammation, and adversely affect overall oyster health. Further investigations regarding fate and sublethal effects of GO are critical to understanding the risks associated with a rapidly growing graphene consumer market.

Mandatory Keywords:

nanomaterials; nanotoxicology; mollusk toxicology; aquatic invertebrates; contaminants of emerging concern

INTRODUCTION

Graphene is a two-dimensional material composed of a single layer of sp^2 hybridized carbon atoms and has unique electrical, mechanical, optical and thermal properties (Zhu et al. 2010; Novoselov et al. 2012). Since its discovery in 2004, graphene has received broad interest in the field of electronics, surface coatings, filtration devices, and biomedicine (Geim and Novoselov 2007). Graphene oxide (GO) is a widely studied graphene derivative and its current uses include transparent conductive films, transistors, sensors, and nanocomposite filters (Goodwin Jr et al. 2018). Commercial use of graphene family nanomaterials (GFNs) is projected to increase exponentially in the next decade as the consumer market for graphene based products continues to grow (Arvidsson et al. 2013). With such widespread use, GFNs will undoubtedly be released into coastal and marine ecosystems as part of the waste stream and, therefore, it is important to study their fate, behavior, and effects on marine biota. With no current information on environmental concentrations of GO and limited toxicity data, potential sublethal adverse effects of exposures to aquatic organisms are poorly understood. Further, it is critical to assess the effects of GO on coastal organisms because marine habitats act as sinks for industrial and anthropogenic contaminants.

Toxicity assessments of nanomaterials in seawater present challenges because of the interactions between particles and their microenvironment, and subsequent changes in particle properties and behavior. Unlike many conventional chemicals, nanomaterials, including GO, do not dissolve in water but rather are suspended in the aqueous solution. Stability of nanomaterials in their environment is based on a variety of factors such as salinity, organic matter, oxidation status, and bioturbation, and together they define the exposure conditions for aquatic biota (Lowry et al. 2012; Jiang et al. 2017). From a toxicological viewpoint, nanomaterial size, shape, and surface properties, along with their chemical composition, are key features to consider for risk assessment (Nel et al. 2006). All of these factors affect bioavailability, uptake, and toxicity to aquatic organisms. Several nanomaterials have been shown to induce oxidative stress in organisms including marine bivalves (Manke et al. 2013; Barbero and Yslas 2016). Oxidative stress arises due to the imbalance in reactive oxygen species (ROS) production and cellular antioxidant capacity. Under such conditions, ROS production begins to overwhelm the cellular antioxidant defensive machinery and cause widespread damage to macromolecules (Kelly et al. 1998). Oxidative stress and direct physical injury have been suggested to play important roles in GO induced toxicity. Zhu et al (2017) reported oxidative damage and involvement of

antioxidant enzymes in the larval stages of *Artemia salina* exposed to GO (Zhu et al. 2017). Zebrafish studies with GO have suggested oxidative and physical damage (Souza et al. 2017). Adverse effects, including developmental nanotoxicity in zebrafish larvae (Wang et al. 2015) as well as behavioral effects in *Artemia* (Mesarič et al. 2015), have been documented in graphene toxicity studies. In the wastewater microbial community, GO was found to affect cell viability and metabolic activity (Ahmed and Rodrigues 2013). To our knowledge, only one study reports the effects of GO exposures in marine bivalves. This recent in vitro work provides evidence for GO toxicity to *Mytilus* hemocytes (Katsumiti et al. 2017). Effects of nanomaterials, such as GO, ideally should be investigated across multiple species in order to identify reliable molecular markers of nanotoxicity in aquatic organisms.

Filter-feeding bivalves, such as *Crassostrea virginica* (Eastern oysters), are commercially important sentinel species and their use as a model for detecting contaminant effects has been well documented (Canesi et al. 2012). Their filtering capacities make them especially valuable for nanotoxicity assessments. Particle size and concentration affect bivalve feeding and filtration rates (Ward et al. 1998; Ward and Shumway 2004) and are essential factors to consider for evaluation of fate and toxicity of nanomaterials. Additionally, intracellular digestion and immune function in bivalves are characterized by processes such as endocytosis and phagocytosis which allows internalization of nano- and micro-scale particles, respectively, in bivalves (Moore 2006). In a dynamic benthic environment, bivalve filter-feeders are exposed to nanomaterials as they aggregate and interact with each other and their surroundings. Therefore, organismal responses are representative of the overall interactive effects of environmental parameters on particle behavior. Bioavailability and toxicity of nanomaterials in aquatic habitats is an emerging area of concern and many critical issues regarding nanomaterial ecotoxicology remain unsolved. Our work is aimed at understanding bivalve responses to GO under environmentally relevant conditions, with the underlying understanding that the toxicity of nanomaterials is associated with changes in particle properties and behavior under exposure conditions. The goal of the present study is to evaluate three types of biomarkers - a cellular damage marker (lipid peroxidation), a toxicity enzyme marker (GST) and a histopathological marker - in GO-exposed Eastern oysters. Digestive gland (DG) and gill tissues were chosen for biomarker assessments. Nanoparticle uptake and effects have been reported in these tissues and the physiological processes associated with them, such as feeding and digestion, can increase bivalve susceptibility to nanotoxicity (Canesi et al. 2012).

METHODS AND MATERIALS

Characterization of GO

X-ray photoelectron spectroscopy (XPS) was used to determine the functional groups on the surface of pristine GO powder (Cheap Tubes Inc.) using a Perkin-Elmer 550 Multi-technique Surface Analyzer (Waltham, Massachusetts). In addition, the morphology of GO in its pristine state was visualized via scanning electron microscopy (SEM) using a ZEISS Sigma VP field emission-scanning electron microscope (Carl Zeiss, Jena, Germany). The hydrodynamic size and surface charge of GO in deionized (DI) water (produced by a Milli-

Q Integral water purification system, ≥ 18.4 MΩ-cm) were estimated by measuring its effective size/size distribution (via a dynamic light scattering (DLS) technique) and zeta (ζ) potential with a ZetaPALS Potential Analyzer (Brookhaven Instruments) using well-established methods (Chowdhury et al. 2013). For DLS analysis, the intensity of scattered light was measured at 90°, and an autocorrelation function was allowed to accumulate for 3 minutes per measurement. The ζ potential was measured using ZetaPALS, which employs phase analysis light scattering (PALS) to measure electrophoretic mobility (EPM) of charged particles. Further, ζ potential values were obtained from EPM using the Smoluchowski model. Each ζ potential measurement was an average of 10 runs, with each run made up of 30 cycles. A GO concentration of 30 mg/L was used for effective size and ζ potential measurements to obtain strong signals. The samples were kept at pH 7 using 0.5 mM phosphate buffer for both measurements, and measurements were conducted in triplicates. Measured samples were made from 200 mg/L GO stock suspensions prepared by dispersing GO powder in DI water via probe sonication (Branson SFX 250, 30 s on/off interval for 1 h).

Experimental design

Oysters were collected from Matunuck Oyster Farm, RI, USA, and acclimated in the laboratory. They were maintained at 21 °C and fed a mixed algal diet consisting of *Tetraselmis*, *Pavlova*, *Chaetoceros* and *Thalassiosira*. GO was purchased from Cheap Tubes Inc. as a 1 g/L suspension of Few Layered Graphene oxide (FLGO, 2–4 layers, >99 wt % purity, 300–800 nm X & Y) in DI water (Table 1). A secondary GO stock of 500 mg/L at 30 ‰ salinity was prepared using 90 ‰ brine and DI water. This stock was probe sonicated for 30 minutes prior to use. Three water tables were used to test control (0), 1, and 10 mg/L GO exposure groups with 8 glass chambers per table containing 0.22 μm filtered natural seawater with a salinity of 30 ‰. For each treatment, 6 replicate glass chambers with 1 oyster per chamber were maintained for the duration of the study. Additionally, each table also contained 2 chambers without oysters to monitor GO concentration and behavior. Immediately after sonication, the secondary stock was introduced into the chambers to achieve a concentration of either 1 or 10 mg/L GO; no GO was added to the control chambers. The final volume in all chambers was 1 L and a water bath was used to maintain the temperature at 20–21 °C. The addition time of GO to each chamber was recorded and 3 renewals were performed each day at 09:30 am, 12:30 pm and 03:30 pm. The study exposure duration was 72 hours with a total of 9 renewals. For each renewal, a new secondary stock was prepared and sonicated, and a new set of chambers was prepared with seawater. Oysters were moved to the new chambers immediately followed by renewal of GO, one chamber at a time. Oysters were fed the mixed algal diet (concentration about 10^6-10^7/mL), as described earlier (75 mL algal cells per oyster per day), every morning before GO was added to the chambers. The chambers were maintained at 16:8 h of light:dark cycle and were sampled daily for temperature, salinity and dissolved oxygen parameters using a YSI meter.

Nanomaterial exposure size and concentration

GO undergoes aggregation and sedimentation in seawater which can further lead to changes in particle size and suspended concentration over time (Chowdhury et al. 2013; Duan et al. 2017; Goodwin Jr et al. 2018). To monitor the size and concentration of GO during the

exposure study, we analyzed samples taken from points approximately 2–3 cm above the bottom (area immediately surrounding the oyster) of all exposure chambers. One minute following the addition of GO stock to the chambers, samples of approximately 2.5 mL were sequentially removed from the chambers at 3-min intervals and placed in glass vials. Sampling order and time were consistent for all analyses to evaluate the effect of time on aggregation. Out of the 2.5 mL water sample, 1 mL was used for DLS analysis using the ZetaPALS, which was started 2 min after each aliquot was removed from its respective beaker. Each DLS analysis lasted for 1 min and care was taken to ensure that the time difference between sample collection and measurement was the same for all chambers. The remainder of the sample was used for GO concentration assessment which was performed on a Biotek Synergy HTX multimode reader using UV/Vis spectroscopy. Concentration of GO in the chambers is expected to decline over time due to filtration by the organism, adherence to surfaces, and sedimentation. Samples were shaken before 200 μL were removed from each vial and absorbance was measured immediately at 230 nm. Samples were read in duplicate in sets of 3 at a time.

Both DLS and concentration assessments were repeated for each chamber upon each renewal throughout the study. For each chamber, there were a total of 9 readings obtained over the course of study. To obtain reliable DLS measurements, only readings with polydispersity index (PDI) <0.4 were used, and the rest were discarded, as per manufacturer's recommendations. Along with effective diameter and polydispersity index, each DLS reading also provides a size distribution curve. From our DLS readings, the one closest to the mean was chosen as a representative for each beaker to generate table 2 for providing information on size distribution and the most abundant sized particle. Additional measurements were carried out on 9 selected samples (2 beakers with oysters and 1 beaker without oysters for each of the 3 test groups) at the end of 3 and 16 h of exposure to assess GO size and its removal from the exposure chambers over time.

Biochemical analyses

At the end of the 72 h exposure duration, oysters were placed in clean seawater for 3 h of depuration prior to harvesting gill and digestive gland tissues. Tissue samples were dissected and immediately frozen at −80 °C for biochemical analyses. All commercial kits were purchased from Sigma-Aldrich and used per manufacturer's instructions.

Lipid peroxidation assay: Lipid peroxidation levels were measured in gill and DG tissues of oysters using a commercial kit purchased from Sigma-Aldrich (MAK085). Damage levels were quantified using malondialdehyde (MDA) standards. Standard curves were generated for every assay run and control charts were maintained to compare blank absorbance, slopes of the curves, and r^2 values. About 25–45 mg of tissue sample was weighed and homogenized on ice in 1:10 weight:volume lysis buffer containing 1% butylated hydroxytoluene. Homogenates were centrifuged at 4 °C at 13,000 g for 10 min. Following centrifugation, 100 μL of supernatant were added to 600 μL thiobarbituric acid and incubated at 95 °C for 1 h in a water bath. Samples were cooled in a bath, centrifuged at 13,000 g at 21 °C for 5 min. Each sample (200 μL) was then analyzed in duplicate in a 96-well microplate at 532 nm using the Biotek Synergy HTX multimode reader. MDA levels

were expressed as nanomoles per gram of wet tissues as well as normalized using total protein levels.

Glutathione-s-transferase activity assay: Glutathione-s-transferase (GST) activity was measured using a spectrophotometric kinetic assay. A commercially available kit from Sigma-Aldrich (CS0410) that utilizes 1-Chloro-2,4-dinitrobenzene (CDNB) as a substrate for GST in the presence of reduced glutathione was used to quantify enzyme activity. The thiol group of glutathione is conjugated to CDNB by GST which leads to a measurable change in absorbance at 340 nm. About 25–45 mg of tissue sample was weighed and homogenized on ice in 10 times the volume of lysis buffer containing 0.4% protease inhibitor cocktail (Sigma Aldrich). Homogenates were centrifuged at 4 °C at 10,000 g for 15 min. Following a 1/5th dilution, samples were introduced in duplicate to a 96-well microplate. A reaction mix containing 9.8 ml of phosphate buffered saline, and 0.1 ml of each of the stock solutions of reduced L-glutathione (200 mM) and CDNB (100 mM) was prepared and added sequentially to the wells containing samples. A diluted GST enzyme control was also analyzed with every run and control charts were maintained to record blank absorbances, slopes of the curves, r^2 values and enzyme activities. Six kinetic readings were recorded for every sample on the Biotek Synergy HTX multimode reader. Rates of change in absorbance were measured to calculate enzyme activities and normalized to total tissue protein levels.

Protein assay: During sample preparation for the GST enzyme activity assay, a subsample of 50 μL was immediately frozen at −20 °C following centrifugation. Frozen samples can undergo one freeze-thaw cycle for protein quantification using a modified Bradford assay (Bradford 1976). A Coomassie (Bradford) protein assay kit (PI23200) from Thermo Scientific was utilized for assessment of total protein levels. The kit relies on the shift in absorbance from 465 nm to 595 nm due to the binding of the dye, in an acidic medium, to proteins in the sample. Bovine serum albumin was used to generate a standard curve for each assay run using a 4-parameter (quadratic) algorithm. Control charts were maintained for each standard curve. Frozen samples were thawed on ice and 10 μL of the sample/standard were placed in duplicate in a 96-well microplate followed by addition of 250 μL of dye. The contents of the plate were mixed by shaking for 30 s and incubated at room temperature for 10 min. Absorbances were measured at 595 nm on the Biotek Synergy HTX multimode reader.

Histopathological analyses: At the end of the 72-hour study period, <5 mm deep gill tissue sections were carefully removed from three oysters and placed in a solution containing 10% formalin in seawater. One randomly chosen replicate oyster from each treatment (control, 1, and 10 mg/L GO) was used for these analyses for preliminary qualitative comparisons of histological effects. These sections were cut sagittally or placed whole (depending on the size of the sample) into cassettes for processing in paraffin. Gill pieces were processed in a sagittal position in the cassette and six- 5 μm serial sections were cut from each block. Sections were stained with hematoxylin and eosin stain (Howard et al. 2004) and examined using a BH51 Olympus compound microscope with photographic

capability. Sections were evaluated for the changes to normal structure of exposed oysters versus controls. Occurrence and severity of changes were described for each treatment.

Statistical analyses: Analysis of variance (ANOVA) was performed using SigmaPlot 13.0 statistical software. Analyses with significant ANOVA p-values were followed by the Student-Newman-Keuls (SNK) pairwise multiple comparison method to determine differences between test groups. Normality and equal variance assumptions were checked for all analyses and a p value of ≤ 0.05 was used to determine significance for ANOVA and post-hoc tests. Error bars in all figures show standard deviation values. Where applicable, Dunn's non-parametric post-hoc test was used as shown in the supplementary information.

RESULTS

GO characterization

SEM analysis showed that the GO particles were mainly aggregated into sheets with lateral sizes in the μm range (Figure 1A). Upon ultrasonic treatment, these aggregates were separated and they remained stable in DI water, as shown by DLS analysis. The effective size of GO, an average of 3 measurements, was 639 nm in DI water. The stability of the DI dispersion of GO is probably due to electrostatic repulsion between the particles as indicated by a ζ potential of −37 mV. The surface charge of GO originates from the ionization of its functional groups such as carboxylic and phenolic moieties, which were confirmed to be present via XPS analysis. A deconvolution of the XPS C1s spectra is shown in Figure 1B where the peaks for sp^2/sp^3 carbon (C–C), epoxide/hydroxyl (C–O–C/C–OH), carbonyl (C=O) and carboxylic (COOH) groups were identified at binding energy (BE) of 284.5 eV, 286.4 eV, 287.7 eV, and 289.4 eV, respectively (Han et al. 2011).

Exposure chamber assessments

The average water temperature, salinity and dissolved oxygen in the exposure chambers were 20.6 ± 0.5 °C, 30.5 ± 0.7 ‰ and 7.3 ± 0.3 mg/L, respectively (n = 12). GO concentrations decreased and particle size increased over time in the chambers with oysters (Figure 2, Tables S1 and S2). Significant relationships between concentration as well as effective diameter and time were observed for chambers with oysters (Figure 2, Table S3). Although concentration and effective diameter measurements for 1 mg/L chambers with oysters were associated with high variation between replicates and fewer reliable size readings with PDI < 0.4 (probably due to low GO concentration/signal), similar trends and significant relationships of time with concentration and effective diameter were noted (Figure 2B, table S3). The r^2 values for concentration and size relationships with time are comparable for 10 mg/L (Figure 2A, $r^2 = 0.91$ for both) as well as for 1 mg/L (Figure 2B, $r^2 = 0.81$ and 0.82, respectively). No GO was detected in any of the control chambers.

Selected beakers were also assessed for changes in the water column at the end of 3 and 16 h. At the end of 3 h, no reliable DLS readings were obtained (polydispersity > 0.4 for all readings due to GO aggregation in seawater), therefore no DLS measurements were taken at the end of 16 h of exposure. For the 10 mg/L chambers with oysters, GO concentration decreased by 25% at the end of 3 h and 84% at the end of 16 h (Figure 3). For chambers

without oysters, the difference in concentration was 3% and 6% after 3 and 16 h, respectively (Figure 3).

The information on size distributions, as shown in Table 2, represents samples removed from the chambers within approximately 1 h of GO addition. These initial measurements suggest that the most abundant sized particles detected in the GO chambers were smaller than the effective diameter. The table also shows that the majority of the particles (particles scoring at least 1 on a distribution scale where the most abundant sized particle is represented by 100 relative units) suspended in the GO chambers are smaller than a micron. However, it must be noted that a wide range of particle sizes was observed in replicate beakers. It must also be noted that 10,000 nm represents the higher size detection limit of the ZetaPALS analyzer. The reported values for effective diameter in Table 2 are indicative of all particles detected in the 1-min long DLS analysis, and that includes these relatively large (near or larger than 10,000 nm) but less abundant particles (<1 relative number on the distribution scale) in the GO chambers. DLS is based on the intensity of light scattered by particles, which is proportional to the sixth power of particle diameter (Barnett 1942). As a result, a very small amount of large GO aggregates can cause a large bias on the effective diameter.

Lipid peroxidation

MDA levels were found to be elevated in the gills of oysters exposed to 10 mg/L GO and unchanged in 1 mg/L GO-exposed oysters (Figure 4, Tables S4 and S5). Results presented here show lipid peroxidation levels based on wet weights as well as normalized using tissue protein concentrations. Gill tissues from oysters exposed to 10 mg/L GO showed higher damage levels when expressed as MDA levels per gram of wet tissue (Figure 4A) and per mg protein (Figure 4B). In the DG tissues, damage levels were found to be significantly elevated in the oysters exposed to 10 mg/L GO, but only when normalized using protein concentrations (Figure 4D). No significant differences in lipid peroxidation levels were observed in oyster DG when expressed as per gram of wet tissues. (Figure 4C).

Glutathione-s-transferase

No significant changes in gill and DG GST activities were observed in GO-exposed oysters (Figure 5, Tables S6 and S7). Normalized GST activities (based on total tissue protein levels) as shown in Figure 5B and 5D were also not significantly different than the controls. A pattern of increase in GST activity in the DG tissues was noted (Figure 5D, tables S6 and S7, ANOVA $p = 0.073$; two tailed t-test p value between control and 10 mg/L= 0.029). Additionally, oyster gill GST, as shown in Figure 5A, showed a declining pattern at 1 mg/L GO when compared to controls (Tables S6 and S7, ANOVA $p = 0.087$; two tailed t-test p value between control and 1 mg/L = 0.015).

Total protein levels

No differences were observed in gill protein levels of oysters exposed to GO. However, protein levels were significantly lower at both GO exposure concentrations in DG tissues (Figure 6, Tables S8 and S9).

Gill histology

Presence of mucous cells in the epithelial lining was noted in the control gill section (Figure 7A). Loss of mucous cells just below the thin surface epithelium was observed in gill sections obtained from GO-exposed oysters (Figure 7B and 7C). The plicae also show increases in the number of hemocytes in vascular spaces as well as among epithelial cells, representing hemocytic infiltration and epithelial hyperplasia in GO-exposed oysters. Elevated numbers of vacuolated cells and interstitial edema in the glandular regions of the gill plicae were also noted. No diseased organisms were identified.

DISCUSSION

GO exposure assessment

In aquatic environments, factors such as ionic strength, salt composition, and natural organic matter affect stability of GO (Chowdhury et al. 2013). GO aggregates in aqueous suspensions and can undergo transformations under natural environmental conditions (Castro et al. 2018) which may affect physicochemical properties (Chowdhury et al. 2013) and, consequently, bioavailability to aquatic organisms. A wide range of nanoparticle sizes maybe available to filter-feeders in the water column because of GO aggregation properties. In our study, the effective diameter of GO increased from 2.6 to 5.6 μm in 46 min in the exposure chambers, as shown in Figure 2A. The broad particle size distribution for these chambers highlights the importance of understanding particle behavior assessments under environmentally relevant conditions. Organic matter in the water column serves as an adsorption phase for GO. Aggregation and sedimentation may slowly remove nanomaterials from the water column (Handy et al. 2008). Additionally, organic material (feces and pseudofeces) from shelled molluscs could increase particle association in the water column. Further, molluscan shells can act as hard surfaces for nanomaterial settlement. Physical disturbances in the water column may resuspend these particles and increase the exposure risks to a variety of organisms. As shown in Figure 3, only 3–6% of GO settled out from the water column in chambers without oysters. In contrast, in just 3 h, 25% of GO was cleared from the 10 mg/L chambers with oysters, and 84% by the end of 16 h. It must be noted that both filtration by the oysters as well as adsorption onto the shell may contribute to the loss of GO from the water column. These findings indicate that in chambers without oysters, in the absence of filtration by the bivalve, most of the GO is still suspended in the water column even after 16 h due to the disturbance and mixing created by chamber aeration. Care was taken to obtain each water sample from 2–3 cm above the bottom of the chamber to ensure that the GO concentration and particle size assessments are representative of changes in the water immediately surrounding the oyster. In natural environments, and as seen in our studies, nanomaterial aggregates can reach micron size ranges (Wong et al. 2010; Sanchís et al. 2015) that are preferred as food by bivalves and other coastal organisms. Ingested particles could also undergo transformation in the digestive tracts of these organisms (McClements et al. 2016) and may further affect feeding and nutritive processes in addition to causing direct damage to internal tissues.

Biochemical assessment

Lipid peroxidation is the process of oxidation of polyunsaturated fatty acids, a primary component of cellular membranes, and can result in altered cell function and cell death (Gutteridge 1995). During lipid peroxidation, numerous reactive intermediates are formed and, until scavenged by antioxidants, such intermediates continue to cause damage and contribute to further ROS generation. The self-propagating nature of lipid peroxidation, and excessive generation of hydroxyl radicals, particularly, poses risks to cellular processes. Our studies show increased MDA levels, a product of lipid peroxidation, in DG and gill tissues of oysters exposed to GO. Similar to our findings, elevated lipid peroxidation and oxidative stress have also been reported in other GO-exposed organisms such as fish (Chen et al. 2016) and polychaetes (De Marchi et al. 2017). Such oxidative damage could be an outcome of cellular internalization of particles leading to elevated ROS production (Manke et al. 2013). GO sheets, similar to other high aspect ratio nanomaterials, have the potential to offer large surface area for particle-cell interactions in biological systems (Lin et al. 2014) and production of ROS. GO has also been demonstrated to result in formation of ROS, such as hydroxyl radical, superoxide radical and singlet oxygen, in an aqueous suspension (Adeleye et al. 2018).

In the present study, lipid peroxidation values are presented as tissue MDA levels based on total wet weight as well as total protein. Generally, normalization using protein levels is regarded as a more robust comparative biomarker assessment. Our results show that both gills and DG tissues have similar trends of increase in oxidative damage in GO-exposed oysters. These findings suggest that lipid peroxidation is a reliable cellular marker of ROS-induced oxidative damage for short-term GO exposures and is a critical endpoint to assess potential outcomes of nanotoxicity of GFNs.

The role of ROS in nanomaterial-induced oxidative stress is also associated with antioxidant and detoxification enzymes (Nel et al. 2006; Manke et al. 2013). Such enzymatic responses include induction of phase II enzymes, such as GST, and can serve as biomarkers of nanotoxicity. GSTs are known for their antiperoxidative potential, involvement in the metabolism of DNA hydroperoxides and reduction of lipid peroxidation products (Bao et al. 1997) as well as in stress signaling (Zhang et al. 2013). Studies documenting GST involvement in signal transduction in nanomaterial toxicity are emerging (Klaper et al. 2009; Zhao et al. 2013). However, reports on changes in activities of GSTs in GO-exposed organisms are scarce. Our studies show no significant differences in GST activities in oysters exposed to GO. However, it must be noted that GST activity patterns (per mg protein) were different between gills and DG. A pattern of increasing activity in DG, possibly due to declining protein levels, and a U-shaped response in gills were observed. We suspect that the short duration of our study is responsible for the lack of significant changes in GST activities. It must also be noted that the response profiles of enzyme biomarkers can often show a bell-shaped trend on a stress gradient (Viarengo et al. 2007). Current information on changes in GST activity patterns in GO-exposed invertebrates (Mesarič et al. 2015; De Marchi et al. 2017) is not sufficient to define the role of GST in GO toxicity. Further investigations need to address these gaps in our understanding of use of enzyme biomarkers in GO toxicity.

Total protein levels in the tissues are a general marker of cellular well-being (Smolders et al. 2004). As mentioned before, they serve as a tool to normalize biomarker data for better comparison and identification of cellular responses and must be considered to examine tissue-specific patterns of cellular changes. Our results show significant declines in protein levels in DG tissues of GO-exposed oysters at both test concentrations. Declines in cellular protein levels could represent tissue damage, direct damage to cellular proteins, and eventual cell death. GO exposure studies have documented decreased cell viability suggesting cytotoxicity at concentrations ≥ 10 mg/L (Ahmed and Rodrigues 2013; Katsumiti et al. 2017). It is also possible that the exposure to nanomaterials affect food uptake, nutrition, and absorption, which in turns leads to decreased protein synthesis and may affect overall organismal energy budgets. Chronic GO exposure studies are required to further determine long-term effects on protein levels.

Histopathological assessment

Finally, we observed histopathological effects of GO exposures in gills. Our representative initial histological assessments of gill tissue damage indicate loss of mucous cells normally lining this portion of the gill, vacuolation and necrosis of plical epithelium alternating with mild hyperplasia of epithelial cells. Additionally, intra-epithelial inflammation, marked inflammation of the underlying connective tissue and sinuses, and multifocal vacuolation of connective tissue were also observed. Mucoid areas of the plica secrete mucous which assists in capturing food particles in the mucous string. Decreased mucous secretion can compromise food capture and lead to nutritive deficiencies and possibly low protein levels, as discussed earlier. Interestingly, the lesions observed in the sections from oysters exposed to 1 mg/L GO appeared more severe than the ones seen in oysters exposed to 10 mg/L GO. This could be partly due to the fact that oysters can close their shells for long durations when the environmental conditions immediately surrounding them are not optimal (Kennedy et al. 1996). Further investigations are required to establish such relationships between GO concentrations and shell closure.

Influx of hemocytes to the gill, as seen in our study, is representative of inflammation. Oyster hemocytes are immune cells that can phagocytose foreign particles and can also produce ROS (Boyd and Burnett 1999). Vertebrate toxicity studies with nanomaterials suggest that cellular internalization of nanomaterials can activate immune cells via cellular redox pathways and trigger inflammation. Further, an interdependent relationship between inflammation and oxidative stress has been suggested in nanomaterial toxicity (Manke et al. 2013). We hypothesize that the sharp edges of GO sheets could induce direct damage to the gill epithelium causing loss of cell membrane integrity which may lead to loss of osmotic balance as well as intra and extracellular edema. Further, as a response to injury, hemocytes infiltrate the epithelium and underlying connective tissues of the gill. Such changes in gills could affect respiration and feeding and can have adverse physiological effects for the organism. In agreement with our findings, other studies have also reported physical damage by GFNs to cellular membranes (Lammel and Navas 2014; Chen et al. 2016) suggesting critical risks to cell function and viability.

Summary

GFN cytotoxicity can be manifested via multiple mechanisms including oxidative stress and ROS-induced damage, physical damage to plasma membranes and other cellular components, and inflammatory response and apoptosis (Ou et al. 2016). Such multiple mechanistic pathways are possibly connected via nanomaterial-induced oxidative stress and associated signal transduction. It is therefore essential to investigate the role and interactions of ROS production, cell signaling pathways and their enzyme biomarkers, and immune function to understand the potential risks associated with GFN exposures. Our study confirms ROS mediated lipid damage as well as an inflammatory response possibly due to physical injury in GO-exposed oysters. With the rapid growth of graphene consumer market, toxicity assessments across multiple aquatic species are essential. As GO studies emerge and molecular initiating events associated with toxicity are identified, further investigations on their physiological implications are also warranted. Additionally, the human health effects of consumption of nanomaterial-exposed oysters as seafood is an area in need of investigation.

Supplementary Material

Refer to Web version on PubMed Central for supplementary material.

ACKNOWLEDGMENT:

The authors would like to acknowledge L. Mills, M. Cantwell and M. Cashman for their contributions towards the review of this manuscript. We would also like to thank P. Raso for the oysters. The present research was performed while B. Khan held an NRC Research Associateship award at the U.S. EPA, ORD/NHEERL, Atlantic Ecology Division.

References

Adeleye AS, Wang X, Wang F, Hao R, Song W, Li Y. 2018 Photoreactivity of graphene oxide in aqueous system: Reactive oxygen species formation and bisphenol a degradation. Chemosphere. 195:344–350. [PubMed: 29274574]

Ahmed F, Rodrigues DF. 2013 Investigation of acute effects of graphene oxide on wastewater microbial community: A case study. Journal of Hazardous Materials. 256–257:33–39.

Arvidsson R, Molander S, Sandén BA. 2013 Review of potential environmental and health risks of the nanomaterial graphene. Human and Ecological Risk Assessment: An International Journal. 19(4): 873–887.

Bao Y, Jemth P, Mannervik B, Williamson G. 1997 Reduction of thymine hydroperoxide by phospholipid hydroperoxide glutathione peroxidase and glutathione transferases. FEBS Letters. 410(2–3):210–212. [PubMed: 9237631]

Barbero CA, Yslas EI. 2016 Ecotoxicity effects of nanomaterials on aquatic organisms: Nanotoxicology of materials on aquatic organisms.

Barnett CE. 1942 Some applications of wave-length turbidimetry in the infrared. The Journal of Physical Chemistry. 46(1):69–75.

Boyd JN, Burnett LE. 1999 Reactive oxygen intermediate production by oyster hemocytes exposed to hypoxia. Journal of Experimental Biology. 202(22):3135–3143. [PubMed: 10539962]

Bradford MM. 1976 A rapid and sensitive method for the quantitation of microgram quantities of protein utilizing the principle of protein-dye binding. Analytical Biochemistry. 72(1):248–254. [PubMed: 942051]

Canesi L, Ciacci C, Fabbri R, Marcomini A, Pojana G, Gallo G. 2012 Bivalve molluscs as a unique target group for nanoparticle toxicity. Marine Environmental Research. 76:16–21. [PubMed: 21767873]

Castro VL, Clemente Z, Jonsson C, Silva M, Vallim JH, de Medeiros AMZ, Martinez DST. 2018 Nanoecotoxicity assessment of graphene oxide and its relationship with humic acid. Environmental Toxicology and Chemistry. 37(7):1998–2012. [PubMed: 29608220]

Chen M, Yin J, Liang Y, Yuan S, Wang F, Song M, Wang H. 2016 Oxidative stress and immunotoxicity induced by graphene oxide in zebrafish. Aquatic Toxicology. 174:54–60. [PubMed: 26921726]

Chowdhury I, Duch MC, Mansukhani ND, Hersam MC, Bouchard D. 2013 Colloidal properties and stability of graphene oxide nanomaterials in the aquatic environment. Environmental Science & Technology. 47(12):6288–6296. [PubMed: 23668881]

De Marchi L, Neto V, Pretti C, Figueira E, Brambilla L, Rodriguez-Douton MJ, Rossella F, Tommasini M, Furtado C, Soares AM. 2017 Physiological and biochemical impacts of graphene oxide in polychaetes: The case of *diopatra neapolitana*. Comparative Biochemistry and Physiology Part C 193:50–60.

Duan L, Hao R, Xu Z, He X, Adeleye AS, Li Y. 2017 Removal of graphene oxide nanomaterials from aqueous media via coagulation: Effects of water chemistry and natural organic matter. Chemosphere. 168:1051–1057. [PubMed: 27816284]

Geim AK, Novoselov KS. 2007 The rise of graphene. Nature Materials. 6(3):183–191. [PubMed: 17330084]

Goodwin DG Jr, Adeleye AS, Sung L, Ho KT, Burgess RM, Petersen EJ. 2018 Detection and quantification of graphene-family nanomaterials in the environment. Environmental Science & Technology. 52(8):4491–4513. [PubMed: 29505723]

Gutteridge J 1995 Lipid peroxidation and antioxidants as biomarkers of tissue damage. Clinical Chemistry. 41(12):1819–1828. [PubMed: 7497639]

Han P, Yue Y, Liu Z, Xu W, Zhang L, Xu H, Dong S, Cui G. 2011 Graphene oxide nanosheets/multi-walled carbon nanotubes hybrid as an excellent electrocatalytic material towards vo2+/vo2+ redox couples for vanadium redox flow batteries. Energy & Environmental Science. 4(11):4710–4717.

Handy RD, Owen R, Valsami-Jones E. 2008 The ecotoxicology of nanoparticles and nanomaterials: Current status, knowledge gaps, challenges, and future needs. Ecotoxicology. 17(5):315–325. [PubMed: 18408994]

Howard DW, Lewis EJ, Keller BJ, Smith CS. 2004 Histological techniques for marine bivalve mollusks and crustaceans. 2nd edition ed. Oxford, MD: NOAA/National Centers for Coastal Ocean Science p. 1–218.

Jiang Y, Raliya R, Liao P, Biswas P, Fortner JD. 2017 Graphene oxides in water: Assessing stability as a function of material and natural organic matter properties. Environmental Science: Nano. 4(7): 1484–1493.

Katsumiti A, Tomovska R, Cajaraville MP. 2017 Intracellular localization and toxicity of graphene oxide and reduced graphene oxide nanoplatelets to mussel hemocytes in vitro. Aquatic Toxicology. 188:138–147. [PubMed: 28521151]

Kelly K, Havrilla CM, Brady TC, Abramo KH, Levin ED. 1998 Oxidative stress in toxicology: Established mammalian and emerging piscine model systems. Environmental Health Perspectives. 106(7):375–384. [PubMed: 9637794]

Kennedy VS, Newell RI, Eble AF. 1996 The eastern oyster: Crassostrea virginica. University of Maryland Sea Grant College.

Klaper R, Crago J, Barr J, Arndt D, Setyowati K, Chen J. 2009 Toxicity biomarker expression in daphnids exposed to manufactured nanoparticles: Changes in toxicity with functionalization. Environmental Pollution. 157(4):1152–1156. [PubMed: 19095335]

Lammel T, Navas JM. 2014 Graphene nanoplatelets spontaneously translocate into the cytosol and physically interact with cellular organelles in the fish cell line plhc-1. Aquatic Toxicology. 150:55–65. [PubMed: 24642293]

Lin S, Wang X, Ji Z, Chang CH, Dong Y, Meng H, Liao Y-P, Wang M, Song T-B, Kohan S. 2014 Aspect ratio plays a role in the hazard potential of ceo2 nanoparticles in mouse lung and zebrafish gastrointestinal tract. ACS nano. 8(5):4450–4464. [PubMed: 24720650]

Lowry GV, Gregory KB, Apte SC, Lead JR. 2012 Transformations of nanomaterials in the environment. Environmental Science & Technology. 46:6893–6899.

Manke A, Wang L, Rojanasakul Y. 2013 Mechanisms of nanoparticle-induced oxidative stress and toxicity. BioMed Research International. 2013:15.

McClements DJ, DeLoid G, Pyrgiotakis G, Shatkin JA, Xiao H, Demokritou P. 2016 The role of the food matrix and gastrointestinal tract in the assessment of biological properties of ingested engineered nanomaterials (ienms): State of the science and knowledge gaps. NanoImpact. 3:47–57. [PubMed: 29568810]

Mesarič T, Gambardella C, Milivojević T, Faimali M, Drobne D, Falugi C, Makovec D, Jemec A, Sepčić K. 2015 High surface adsorption properties of carbon-based nanomaterials are responsible for mortality, swimming inhibition, and biochemical responses in *artemia salina* larvae. Aquatic Toxicology. 163:121–129. [PubMed: 25889088]

Moore M 2006 Do nanoparticles present ecotoxicological risks for the health of the aquatic environment? Environment International. 32(8):967–976. [PubMed: 16859745]

Nel A, Xia T, Mädler L, Li N. 2006 Toxic potential of materials at the nanolevel. Science. 311(5761): 622–627. [PubMed: 16456071]

Novoselov KS, Fal V, Colombo L, Gellert P, Schwab M, Kim K. 2012 A roadmap for graphene. Nature. 490(7419):192–200. [PubMed: 23060189]

Ou L, Song B, Liang H, Liu J, Feng X, Deng B, Sun T, Shao L. 2016 Toxicity of graphene-family nanoparticles: A general review of the origins and mechanisms. Particle and Fibre Toxicology. 13(1):1–24. [PubMed: 26746196]

Sanchís J, Olmos M, Vincent P, Farré M, Barceló D. 2015 New insights on the influence of organic co-contaminants on the aquatic toxicology of carbon nanomaterials. Environmental science & technology. 50(2):961–969. [PubMed: 26694946]

Smolders R, Bervoets L, De Coen W, Blust R. 2004 Cellular energy allocation in zebra mussels exposed along a pollution gradient: Linking cellular effects to higher levels of biological organization. Environmental Pollution. 129(1):99–112. [PubMed: 14749074]

Souza JP, Baretta JF, Santos F, Paino IMM, Zucolotto V. 2017 Toxicological effects of graphene oxide on adult zebrafish (*danio rerio*). Aquatic Toxicology. 186:11–18. [PubMed: 28242497]

Viarengo A, Lowe D, Bolognesi C, Fabbri E, Koehler A. 2007 The use of biomarkers in biomonitoring: A 2-tier approach assessing the level of pollutant-induced stress syndrome in sentinel organisms. Comparative Biochemistry and Physiology Part C. 146(3):281–300. [PubMed: 17560835]

Wang ZG, Rong Z, JIANG D, Jing ES, Qian X, Jing S, CHEN YP, Xin Z, Lu G, LI JZ. 2015 Toxicity of graphene quantum dots in zebrafish embryo. Biomedical and Environmental Sciences. 28(5): 341–351. [PubMed: 26055561]

Ward J, Levinton J, Shumway S, Cucci T. 1998 Particle sorting in bivalves: In vivo determination of the pallial organs of selection. Marine Biology. 131(2):283–292.

Ward JE, Shumway SE. 2004 Separating the grain from the chaff: Particle selection in suspension-and deposit-feeding bivalves. Journal of Experimental Marine Biology and Ecology. 300(1–2):83–130.

Wong SW, Leung PT, Djurišić A, Leung KM. 2010 Toxicities of nano zinc oxide to five marine organisms: Influences of aggregate size and ion solubility. Analytical and bioanalytical chemistry. 396(2):609–618. [PubMed: 19902187]

Zhang M, An C, Gao Y, Leak RK, Chen J, Zhang F. 2013 Emerging roles of nrf2 and phase ii antioxidant enzymes in neuroprotection. Progress in neurobiology. 100:30–47. [PubMed: 23025925]

Zhao Y, Wu Q, Li Y, Wang D. 2013 Translocation, transfer, and in vivo safety evaluation of engineered nanomaterials in the non-mammalian alternative toxicity assay model of nematode caenorhabditis elegans. Rsc Advances. 3(17):5741–5757.

Zhu S, Luo F, Chen W, Zhu B, Wang G. 2017 Toxicity evaluation of graphene oxide on cysts and three larval stages of *artemia salina*. Science of the Total Environment. 595:101–109. [PubMed: 28380404]

Zhu Y, Murali S, Cai W, Li X, Suk JW, Potts JR, Ruoff RS. 2010 Graphene and graphene oxide: Synthesis, properties, and applications. Advanced Materials. 22(35):3906–3924. [PubMed: 20706983]

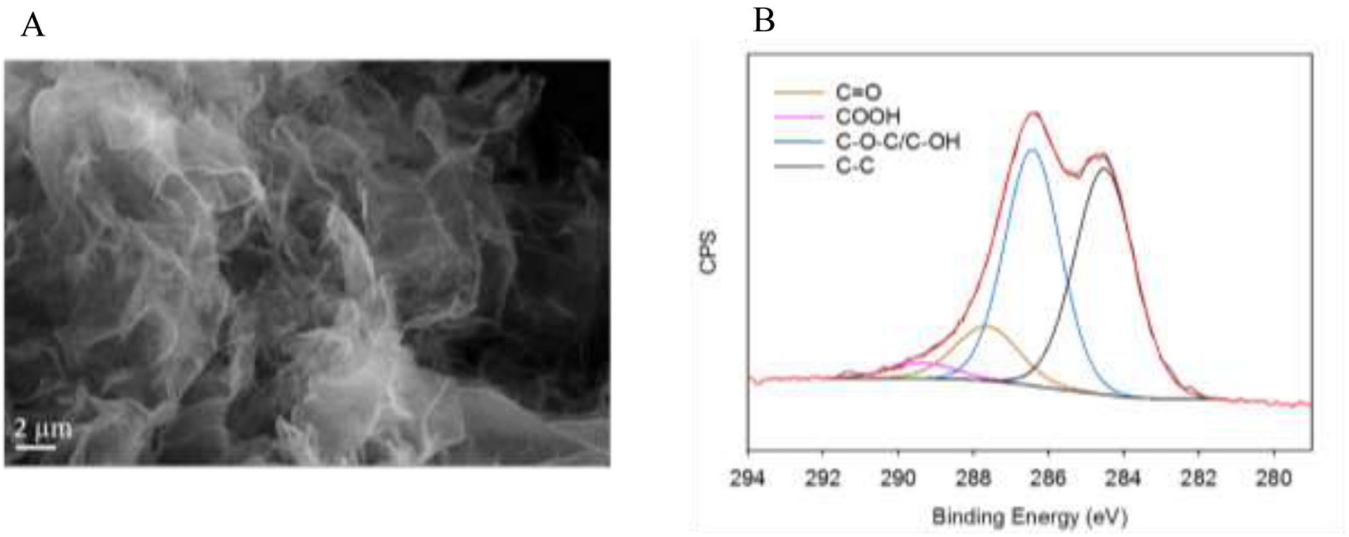

Figure 1.

Physicochemical characterization of GO used in the present investigation: (A) Scanning electron micrograph, and (B) deconvoluted C1s spectrum of the pristine GO particles showing binding energies on the x-axis and counts per second (CPS) on the y-axis.

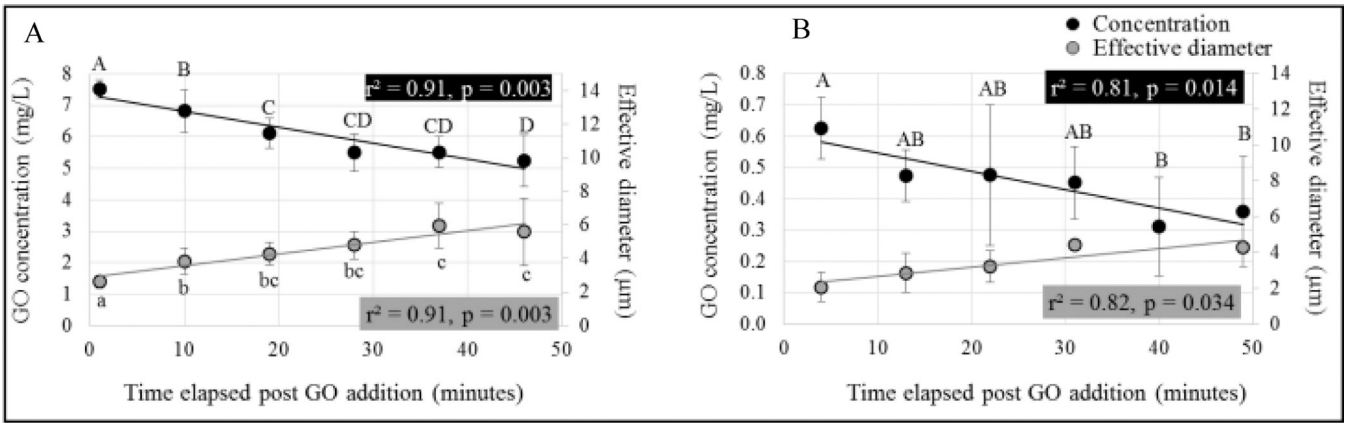

Figure 2.

Relationship of time with the measured concentration and effective diameter for (A) 10 mg/L and (B) 1 mg/L GO exposure chambers containing oysters. Black circles represent mean concentration measurements and are plotted on the primary y-axis (n = 8 per data point); grey circles represent effective diameter and are plotted on the secondary y-axis (n = 4–8 per data point in 10 mg/L chambers, n =1–5 per data point for 1 mg/L chambers). Standard deviations, regression r^2 and p values are indicated. Different letters represent significant differences.

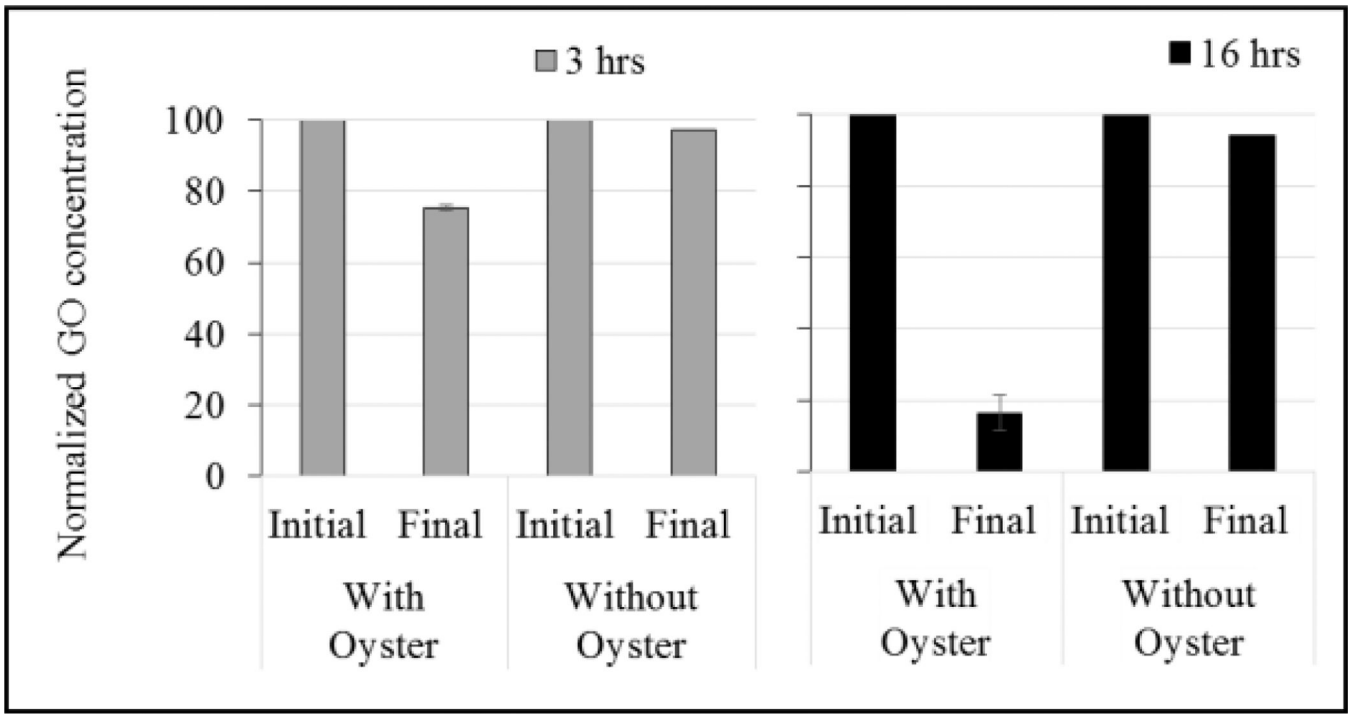

Figure 3.

Initial and final measured GO concentrations after 3 and 16 hours in the 10 mg/L GO chambers with and without oysters; n = 2 for chambers with oysters and n = 1 for chambers without oysters. Values are normalized to the initial GO concentration in the chamber and are expressed as percentages.

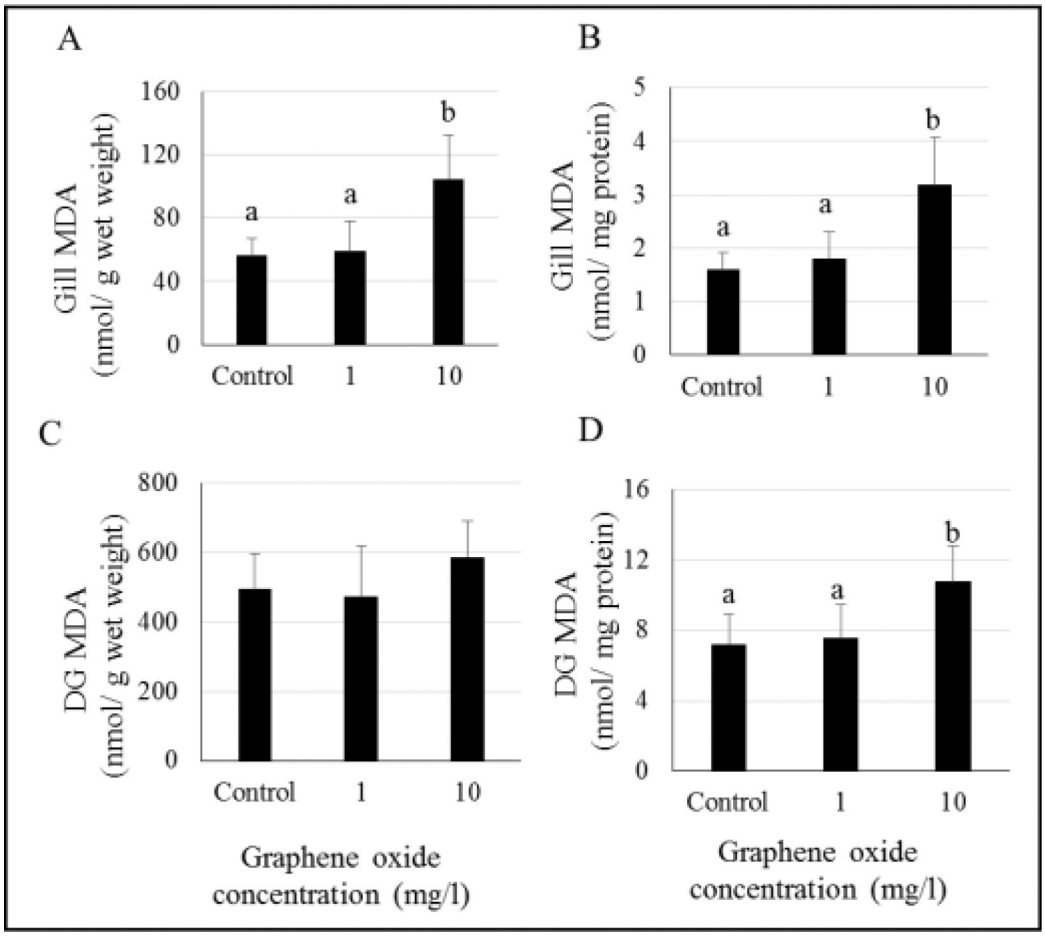

Figure 4.

Malondialdehyde (MDA) levels in gill (A and B) and digestive gland (DG) (C and D) tissues of GO-exposed oysters. Different letters indicate significant differences; no letters indicate no differences.

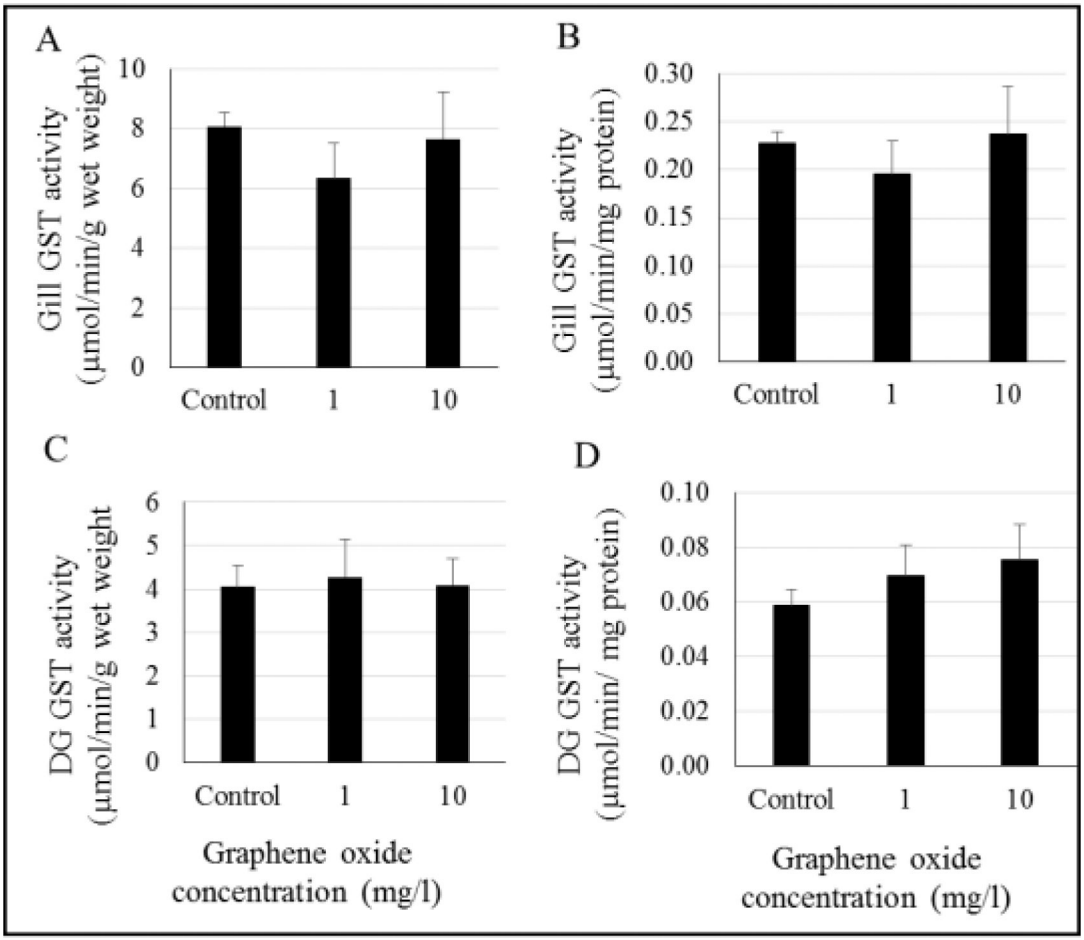

Figure 5.

Activity of glutathione-s-transferase (GST) in gill (A and B) and digestive gland (DG) (C and D) tissues of GO-exposed oysters. No significant differences were found.

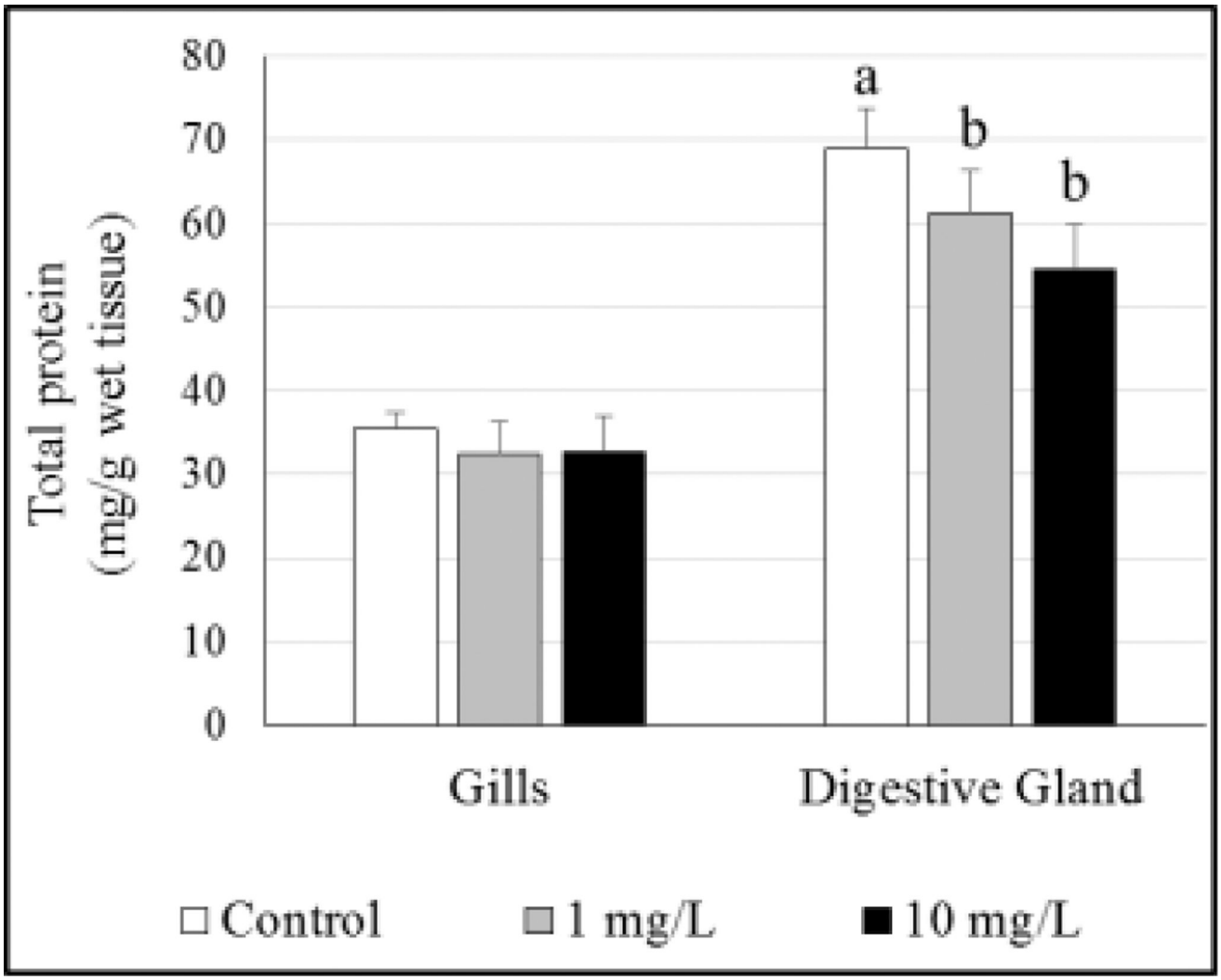

Figure 6.
Total protein levels in gill and digestive gland tissues of GO-exposed oysters. Different letters indicate significant difference between concentrations, no letters indicate no differences.

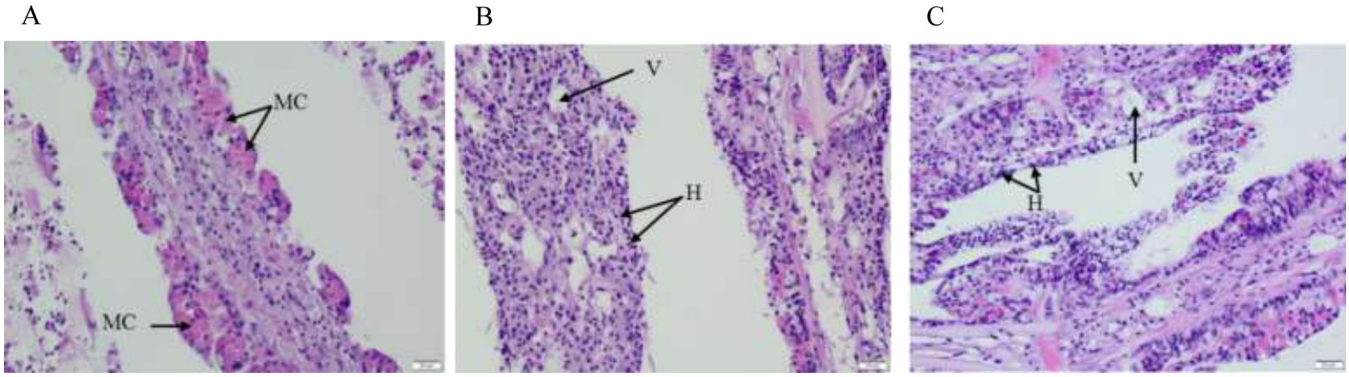

Figure 7.

Histological gill tissue sections from (A) control, (B) 1 mg/L GO-exposed, (C) 10 mg/L GO-exposed oysters. In control animals, mucus cells are abundant in the epithelium and minimal numbers of hemocytes are noted in the underlying connective tissues and vessels. GO-exposed animals show a loss of mucus cells, loss of non-mucus epithelial cells, destruction of underlying connective tissues and diffuse severe hemocytic inflammation. MC - mucous cells, H - hemocytes, V – vacuolation. The scale bar represents 20 μm.

Table 1.

Summary of the characterization of GO used in this investigation.

Property	Value
Lateral size[a]	300 – 700 nm
Number of layers[a]	2 – 4
Thickness[a]	1.4 – 4.8 nm
Carbon/Oxygen ratio	1.55
Hydrodynamic diameter	638.6 ± 23.4 nm
Zeta potential[b]	−37.1 ± 2.4 mV

[a]Information provided by the manufacturer

[b]Ionic strength was adjusted to 1 mM (NaCl)

Table 2.

Concentration and particle size information from 10 mg/L and 1 mg/L GO chambers. The most abundant particle size in the sample is assigned a relative number of 100 during DLS measurements. Size distribution is shown as a range associated with particles assigned a relative number of at least 1 (data >1), and also as a range associated with particles assigned any number > 0 (all data). Chambers indicated as SW are seawater chambers without oysters.

10 mg/L				**Size range (relative distribution)**		
Chamber #	**Time post GO addition**	**Conc**	**Most abundant size**	**Data >1**	**all data**	**Effective diameter**
	mins	**mg/L**	**nm**	**nm**	**nm**	**nm**
1	1	7.41	284	284–2405	284–10,000	2453.8
4	10	5.88	764	514–764	514–10,000	3778
7	19	5.81	77	77–108	77–10,000	4730.7
10	28	5.84	112	112–179	112–10,000	4762.4
13	37	4.83	167	145–224	145–6452	5281.5
16	46	6.12	68	68–95	68–10,000	4930.6
19 (SW)	55	6.94	126	126-	126–7315	5005.6
22 (SW)	64	5.96	120	120–1096	120–10,000	5824.6
1 mg/L				**Size range (relative distribution)**		
Chamber #	**Time post GO addition**	**Conc**	**Most abundant size**	**data >1**	**all data**	**Effective diameter**
	mins	**mg/L**	**nm**	**nm**	**nm**	**nm**
2	4	0.42	469	469–691	469–5303	2350.8
5	13	0.35	781	715–8387	715–10,000	2999.5
8	22	0.93	168	146–1392	146–10,000	3307.4
11	31	0.63	105	89–808	89–10,000	4406.3
14	40	0.23	64	64-	64–10,000	12438.4
17	49	0.74	127	127–728	127–10,000	4269.8
20 (SW)	58	0.3	2786	2736–2820	2736–2820	3447
23 (SW)	67	0.25	437	168–500	168–7617	3848.6